

This document is confidential and is proprietary to the American Chemical Society and its authors. Do not copy or disclose without written permission. If you have received this item in error, notify the sender and delete all copies.

Engineered Coalescence by Annealing of 3D Ge Microstructures into High-Quality Suspended Layers on Si

Journal:	<i>ACS Applied Materials & Interfaces</i>
Manuscript ID:	am-2015-05054u.R1
Manuscript Type:	Article
Date Submitted by the Author:	n/a
Complete List of Authors:	Salvalaglio, Marco; Università degli Studi di Milano-Bicocca, L-NESS and Department of Materials Science Bergamaschini, Roberto; Università degli Studi di Milano-Bicocca, L-NESS and Department of Materials Science Isa, Fabio; ETH Zurich, Solid State Physics Scaccabarozzi, Andrea; Università degli Studi di Milano-Bicocca, L-NESS and Department of Materials Science Isella, Giovanni; Politecnico di Milano, L-NESS and Department of Physics Backofen, Rainer; Technische Universität Dresden, Institut für Wissenschaftliches Rechnen Voigt, Axel; Technische Universität Dresden, Institut für Wissenschaftliches Rechnen Montalenti, Francesco; Università degli Studi di Milano-Bicocca, L-NESS and Department of Materials Science Capellini, Giovanni; IHP Microelectronics, ; Università Roma Tre, Department of Science Schroeder, Thomas; IHP Microelectronics, Von Kanel , Hans; ETH Zurich, Solid State Physics Miglio, Leo; Università degli Studi di Milano-Bicocca, L-NESS and Department of Materials Science

SCHOLARONE™
Manuscripts

This document is the Accepted Manuscript version of a Published Work that appeared in final form in ACS Applied Materials & Interfaces, copyright © American Chemical Society after peer review and technical editing by the publisher. To access the final edited and published work see ACS Appl. Mater. Interfaces 2015, 7, 34, 19219–19225
<https://pubs.acs.org/doi/abs/10.1021/acsami.5b05054>

1
2
3
4
5
6
7
8
9
10
11
12
13
14
15
16
17
18
19
20
21
22
23
24
25
26
27
28
29
30
31
32
33
34
35
36
37
38
39
40
41
42
43
44
45
46
47
48
49
50
51
52
53
54
55
56
57
58
59
60

Engineered Coalescence by Annealing of 3D Ge Microstructures into High-Quality Suspended Layers on Si

Marco Salvalaglio¹, Roberto Bergamaschini¹, Fabio Isa², Andrea Scaccabarozzi¹, Giovanni Isella³, Rainer Backofen⁴, Axel Voigt⁴, Francesco Montalenti¹, Giovanni Capellini^{5,6}, Thomas Schroeder⁵, Hans von Känel², Leo Miglio^{1,}*

¹L-NESS and Department of Materials Science, Università di Milano-Bicocca
Via R. Cozzi 55, I-20126, Milano, Italy

²Laboratory for Solid State Physics, ETH Zürich
Otto-Stern-Weg 1, CH-8093, Zürich, Switzerland

³L-NESS and Department of Physics, Politecnico di Milano
Via F. Anzani 42, I-22100 Como, Italy

⁴Institut für Wissenschaftliches Rechnen, Technische Universität Dresden
Zellescher Weg 12-14, D-01069, Dresden, Germany

⁵IHP
Im Technologiepark 25, D-15236, Frankfurt (Oder), Germany

⁶Department of Science, Università Roma Tre
Viale Marconi 446, I-00146, Roma, Italy

*Corresponding Author: leo.miglio@unimib.it

1
2
3 ABSTRACT: The move from dimensional to functional scaling in microelectronics leads to
4 renewed interest towards integration of Ge on Si. In this work, simulation-driven experiments
5 leading to high-quality suspended Ge films on Si pillars are reported. Starting from an array of
6 micrometric Ge crystals, the film is obtained by exploiting their temperature-driven coalescence
7 across nanometric gaps. The merging process is simulated by means of a suitable surface-
8 diffusion model within a phase-field approach. The successful comparison between experimental
9 and simulated data demonstrates that the morphological evolution is purely driven by the
10 lowering of surface-curvature gradients. This allows for a fine control over the final morphology.
11 At fixed annealing time and temperature, perfectly merged films are obtained from Ge crystals
12 grown at low temperature (450°C), while some void regions are still persistent for crystals grown
13 at higher temperature (500°C), due to their different initial morphology. The latter condition,
14 however, looks very promising for possible applications. Indeed, Scanning Tunneling Electron
15 Microscopy (STEM) and High Resolution - Transmission Electron Microscopy (HR-TEM)
16 analyses show that, at least during the first stages of merging, the developing film is free from
17 threading-dislocations. The present findings, thus, introduce a promising path to integrate Ge
18 layers on Si with a low dislocation density.
19
20
21
22
23
24
25
26
27
28
29
30
31
32
33
34
35
36
37
38
39
40
41
42
43

44 KEYWORDS: heteroepitaxy, semiconductors, substrate patterning, surface diffusion,
45 dislocations
46
47
48
49
50
51
52
53
54
55
56
57
58
59
60

1. INTRODUCTION

Fostered by the move from dimensional to functional scaling in microelectronics,^[1] germanium has been recently re-investigated as a possible high-mobility replacement for mainstream silicon MOSFET technology.^[2] However, the material growth challenges in heterogeneous integration on Si are substantial, because of the 4% lattice misfit: any Ge film on Si will relax through the formation of misfit dislocations, because the critical thickness for such a large misfit is only a few monolayers. To accommodate the lattice mismatch between the two materials, a thick Si_{1-x}Ge_x graded layer can be grown between the silicon substrate and the active germanium layer, so that the defect density is significantly reduced, but still not eliminated.^[3] To mitigate this problem, several alternatives have been investigated. In particular, the aspect-ratio-trapping process for growing Ge and SiGe buffer layers within narrow oxide trenches, patterned on silicon substrates at sub-micron distances^[4,5] and, very recently, the use of composite AlAs/GaAs buffer layers.^[6]

To date, the high-quality integration of Ge on Si beyond the nanometer scale, with no threading dislocations reaching the top part of crystals, has been achieved only in the form of vertical, micron-sized Ge structures grown on deeply-patterned Si substrates [7,8]. As demonstrated and discussed in refs [7,9,10], full pyramidal faceting at the top regions allows for a complete lateral expulsion of threading dislocations (instead present when considering flat top), leading to several microns of defect-free material. Extending such properties to a planar film would lead to substrates for microelectronic applications with unprecedented quality.

In this work we show that a perfect array of such Ge crystals can lead to the formation of a single suspended Ge layer through a lateral merging process. This is demonstrated by simulation-driven experiments, followed by an extensive morphological and structural characterization. A detailed

1
2
3 theoretical interpretation of the merging process is also provided and critical issues in terms of
4 material quality are discussed.
5
6
7
8
9

10 **2. EXPERIMENTAL SECTION**

11
12 **2.1 LEPECVD crystal growth and in-situ annealing.** The epitaxial growth of micrometric Ge
13 crystals, used as starting point for the annealing process, is performed by Low Energy Plasma
14 Enhanced Chemical Vapor Deposition (LEPECVD). In this epitaxial technique, the molecules of
15 the precursor gas, germane, are activated by a low-energy (~ 10 eV), magnetically confined Ar
16 plasma, enabling the deposition of Ge crystals at low growth temperature (400 – 550 °C) and
17 high growth rate (up to 10 nm/s).^[11] Prior to the epitaxial growth, patterned Si substrates are
18 treated by the RCA cleaning,^[12] dipped in 5% HF solution for 30 s and rinsed in de-ionized water
19 for 3 min. Afterwards, the substrates are loaded into the LEPECVD load-lock reaching a
20 pressure of $\sim 10^{-8}$ mbar and finally transported into the growth chamber (base pressure of 1×10^{-9}
21 mbar) and heated up at 300 °C for 15 min before reaching the growth temperature.
22
23
24
25
26
27
28
29
30
31
32
33
34
35

36 In particular, the different samples considered here consist of 8 μm tall Ge crystals grown by
37 LEPECVD at 450 or 500 °C \pm 15 °C, at a rate of 4.2 nm/s and with a chamber pressure of
38 3×10^{-2} mbar. After the epitaxial growth, an annealing treatment is performed in-situ in the
39 growth chamber (pressure of 5×10^{-7} mbar), heating the sample to 800 °C (the highest attainable
40 annealing temperature allowed in our apparatus), at a rate of 2 °C/s. The annealing time is
41 measured starting when the sample reaches the temperature of 800 ± 10 °C. Thermal cycles are
42 also performed in some cases by repeatedly varying the temperature between 600 and 800 °C
43 with a heating ramp of 1 °C/s and cooling at 2 °C/s.
44
45
46
47
48
49
50
51
52
53
54
55
56
57
58
59
60

1
2
3 **2.2 Morphology analysis.** The morphology of the as-grown and annealed Ge crystals is
4 investigated by means of Atomic Force Microscopy (AFM) using an Asylum Research MFP-3D
5 and Scanning Electron Microscopy (SEM) using a Zeiss ULTRA 55 digital field emission
6 apparatus. The density of threading dislocations in the Ge crystals and in the planar unpatterned
7 area is inferred by selective defect etching and etch-pit counting by means of AFM, SEM and
8 Nomarski microscopy (Nikon Eclipse 200D) on an area of at least $500 \times 500 \mu\text{m}^2$. The etching
9 procedure consists of dipping the Ge samples into a Iodine-based solution (15 mg I_2 , 33 ml
10 glacial acetic acid, 10 ml 65% nitric acid, 5 ml 40% HF) for 40 s at 0°C .^[13] The quality of the
11 merged region is assessed by Scanning Tunneling Electron Microscopy (STEM), and High
12 Resolution - Transmission Electron Microscopy (HR-TEM) using a FEI Tecnai Osiris system.
13
14
15
16
17
18
19
20
21
22
23
24
25
26

27 **2.3 Phase-field simulations.** The process of merging of adjacent Ge crystals is investigated by
28 means of numerical simulations based on a phase-field approach (see ref [14] for a review),
29 which permits three-dimensional (3D) domains to be easily managed, and naturally accounts for
30 complex topological changes. The surface profile is implicitly tracked by means of an order
31 parameter φ varying continuously from 1 inside the solid to 0 outside, as given by $\varphi(\mathbf{x}) =$
32 $0.5[1 - \tanh(3d(\mathbf{x})/\varepsilon)]$, where ε is the interface width and d is the signed-distance from the
33 profile of the surface, located at $\varphi = 0.5$. In Figure 1a, the $\varphi = 0.5$ iso-surface corresponding to
34 a Ge crystal is shown. According to the Onsager linear law, material transport is described by
35 $\partial\varphi/\partial t = \nabla \cdot [M(\varphi, \mathbf{x})\gamma\nabla\kappa]$ where $\kappa = \kappa(\varphi(\mathbf{x}))$ accounts for the local curvature of the surface,
36 and γ is the surface energy density, here assumed to be isotropic as faceting is not found to play
37 a crucial role (see Supporting Information, where surface anisotropy is tackled by exploiting the
38 method introduced in ref [15]). Finally, M is the mobility function, restricted to the surface by
39 the typical setting $M = M_0(36/\varepsilon)\varphi^2(1 - \varphi)^2$ where M_0 is a scaling factor, forced to be zero
40
41
42
43
44
45
46
47
48
49
50
51
52
53
54
55
56
57
58
59
60

1
2
3 inside the Si region ($M_0 \sim 0$, see Figure 1b) in order to account for the stability of the Si pillars
4 at the annealing temperatures^[16]. The isotropic surface energy γ is chosen to be unitary, so that
5 the simulation time scale is directly determined by M_0 only. Numerical simulations are
6 performed by using the Finite Element Method toolbox AMDiS.^[17,18] Local mesh refinement is
7 adopted in order to improve the spatial resolution in the region where $\varphi = 0.5$, i.e. at the surface
8 of the solid phase (Figure 1c). This space adaptivity allows the details of the surface to be
9 accurately defined while minimizing the computational cost. A semi-implicit integration scheme
10 is implemented. The boundary conditions are set to be periodic in the $[110]$ and $[1\bar{1}0]$ directions,
11 while zero-flux Neumann boundaries are imposed in the $[001]$ direction, i.e. at the top and
12 bottom of the simulation cell. Both sequential and parallel executions are considered with direct
13 and iterative solvers. Further details are reported in the Supporting Information.
14
15
16
17
18
19
20
21
22
23
24
25
26
27
28
29
30
31

32 3. RESULTS AND DISCUSSION

33
34 **3.1 Morphological evolution.** As illustrated in refs [7] and [8] the epitaxial growth of Ge onto
35 an array of microns-tall Si pillars in a highly kinetic regime may result in closely-spaced
36 individual Ge crystals, separated by gaps as large as tens of nanometers. This particular 3D
37 morphology results from the combined effect of a short diffusion length, ensured by the high
38 deposition rate (~ 4 nm/s) of LEPECVD at comparatively low temperatures ($\sim 450 - 500$ °C),
39 and mutual shielding of the reactive gas flux by neighboring crystals. A typical pattern consists
40 of 8 μm tall Si pillar, spaced by a few micrometers as shown in Figure 2a for the specific case of
41 $2 \times 2 \mu\text{m}^2$ Si pillar with 2 μm trench. A perspective SEM view of an as-grown 8 μm tall Ge crystal
42 on top of a $2 \times 2 \mu\text{m}^2$ Si pillar is shown in Figure 2b. The crystal is bounded by $\{110\}$ sidewalls
43 and $\{113\}$ and $\{111\}$ top facets, typical at the temperature of 500 °C and for the present Si pillar
44
45
46
47
48
49
50
51
52
53
54
55
56
57
58
59
60

1
2
3 size. An additional (001) surface facet is usually found on crystals grown at lower temperature,
4
5 or on larger Si pillars^[8] (see below). This morphological feature is important since only as-
6
7 grown crystals with fully slanted facets at the growth front were shown to be free of threading
8
9 dislocations, ^[7,9,10] without the need for post-growth annealing which is usually performed on
10
11 planar substrates to improve the crystal quality. However, the morphology of these Ge crystals
12
13 does change upon annealing, as indicated in the SEM and AFM images of Figure 2c. These
14
15 images were obtained after six thermal cycles between 600 and 800 °C, each one lasting for 6
16
17 min. Evidently, the annealing causes smoothening of the edges between the {113} facets and
18
19 flattening of the top cusp towards a (001) facet, indicating that the morphology is beginning to
20
21 evolve towards equilibrium. In the absence of deposition, the changes in the profile must be
22
23 attributed to material redistribution driven by the tendency of the system to minimize its free
24
25 energy. Since the Ge crystals are strain-free^[7,9,10] the morphological changes must be driven by
26
27 surface energy lowering. Bulk diffusion can be excluded at the annealing temperatures in view of
28
29 its high activation barrier.^[19]

30
31
32 Based on these considerations we have developed a 3D surface diffusion model, where the
33
34 chemical potentials are derived by the local curvature,^[20] implemented in a suitable phase-field
35
36 framework, in order to describe the morphological evolution during the annealing process.
37
38 Details of the model are provided in the Experimental Section and in the Supporting Information.
39
40 We did not include any facet-dependent surface energy, which greatly simplifies the model, with
41
42 no loss of predictive power (as demonstrated in the Supporting Information). Since the average
43
44 mobility M_0 of Ge along the surface profile cannot be predicted by calculations, we use it as a
45
46 free parameter to quantitatively match the experimental time scale. Annealing simulations based
47
48 on this description are quite effective in capturing the initial edge smoothening at the top of the
49
50
51
52
53
54
55
56
57
58
59
60

1
2
3 Ge crystal, as reported in the lower inset of Figure 2c. By extending the simulations to much
4 longer annealing times, a global rounding of the Ge crystal profile is obtained, with significant
5 lateral expansion. This is illustrated in Figure 3a, where snapshots of a prolonged annealing
6 simulation are reported. The morphological change can be interpreted as being caused by
7 significant material fluxes from the top and the vertical edges to the center of the sidewalls (as
8 indicated by red arrows), in order to equilibrate the local surface curvature which, in turn,
9 determines the chemical potential. To better appreciate the extent of such a process, cross-section
10 and top views of the crystals are compared for the initial and the final stage of the simulation in
11 Figure 3b.
12
13
14
15
16
17
18
19
20
21
22
23

24 As already mentioned, adjacent Ge crystals grown in such conditions on Si pillars spaced two
25 microns, are separated by gaps of just a few dozen nanometers.^[7,8] Therefore, we expect that, for
26 long enough post-growth annealing times, neighboring Ge crystals will touch in the upper part
27 and gradually merge, eventually resulting in a flat suspended Ge layer on top of the Si pillars. In
28 order to verify this assumption, in-situ annealing experiments were performed at increasing times
29 up to 60 min at 800 °C. Figure 4 illustrates the morphology evolution of 8 μm tall Ge crystals on
30 top of 8 μm Si pillars. Top (a) and lateral (b) SEM images, as well as AFM perspective views (c-
31 f) of the tops of crystals are reported for different durations of the annealing process (additional
32 data are provided in Figure S1 in the Supporting Information). The initial individual crystals
33 obtained after the LEPECVD growth at 450 °C for 2×2 μm² Si pillars spaced by 2 μm exhibit a
34 top (001) facet and are spaced ~ 150 nm apart. Similar to the isolated structures of Figure 2, the
35 crystals assume a rounded shape after an annealing time of 5 min (Figure 4a). Some of them are
36 already touching at this stage and eventually merge along the <110> directions (10 and 20 min),
37 while sizeable undulations at the top remain along with a regular array of holes at the crossing of
38
39
40
41
42
43
44
45
46
47
48
49
50
51
52
53
54
55
56
57
58
59
60

1
2
3 the original Si trenches. It is evident from the enlarged AFM scan of a single Ge crystal annealed
4 for 10 min, reported in Figure 4d, that the original facets have blurred to an almost continuous
5 smooth profile with a large density of surface steps, probably resulting in a slow-down of the
6 surface mobility. Finally, after an annealing time of 60 min, the holes are closed and a
7 continuous film is obtained (see Figures 4). The AFM scans indicate a peak-to-valley amplitude
8 of about 250 nm, still phase-matched to the underlying pattern of Si pillars.

9
10
11 In order to obtain a deeper insight into the diffusion mechanisms leading to the observed
12 morphological changes, simulations for dense arrays are performed, with the same geometric
13 parameters as for the experimental case of Figure 4, but, with no loss of generality, for the
14 slightly rounded initial shape indicated in Figure 2c. Figure 5a shows that the initial lateral
15 expansion due to thermal treatment of crystals quickly reduces their distance so that they touch.
16
17 At the onset of merging, here corresponding to an annealing time of $t = 2$ min, the contact region
18 has almost circular cross-section, and acts as a collector for neighboring material due to
19 differences in the local curvature (see Figure S2 in the Supporting Information). The expansion
20 of these regions allows the system to reduce its surface energy. Simultaneously, Ge material
21 originating from the lower part of the sidewalls is found to move upwards in kind of a zipping
22 action further closing the trenches between the crystals. A thick suspended film with holes
23 located at the crossings of the trenches is then formed ($t = 10$ min). At this stage the structure is,
24 however, not yet in equilibrium, as the holes provide a gradient in the local curvatures, so that Ge
25 is collected from both the top and the bottom of the crystals until the holes are completely closed.
26
27 This leaves an undulated surface profile of the resulting film at $t = 50$ min, which slowly flattens
28 until $t = 100$ min. This prediction nicely agrees with the experimental behavior observed in
29
30
31
32
33
34
35
36
37
38
39
40
41
42
43
44
45
46
47
48
49
50
51
52
53
54
55
56
57
58
59
60

1
2
3 Figures 4 (see also the movie in the Supporting Information). We therefore conclude that the
4 surface curvature is the main driving force leading to the coalescence of the crystals.
5
6

7
8 Such a mechanism is valid in general, provided that the crystal aspect-ratio is sufficiently large
9 that the initial lateral expansion causes bridging of the gaps somewhere. In order to prove this,
10 we considered different patterns, both in experiments and simulations. In Figure 6a we show the
11 annealing results, after 5 and 60 min, of 8 μm tall Ge crystals grown on a pattern of $2 \times 2 \mu\text{m}^2$ Si
12 pillars separated by 3 μm wide trenches, leading to a distance of ~ 300 nm in their as-grown
13 state. Due to the larger gap, the lateral expansion after an annealing time of 5 min is not
14 sufficient to create a bridge. Instead, only rounding of the crystals is observed, both in
15 experiments and simulations. Only upon extending the annealing time to 60 min it is possible to
16 see the onset of crystal merging. This delay in the full coalescence is observed also in the
17 simulations, although it is not as long. Possibly, the slower experimental evolution is due to
18 dense step-bunching already seen in the AFM scan of Figure 4e. The effect of a different lateral
19 size of the Si pillars is, instead, shown in Figure 6b (see also Figure S3-S5 in the Supporting
20 Information). Here, $5 \times 5 \mu\text{m}^2$ Si pillars are seen to lead to the formation of Ge crystals with a
21 much wider (001) top facet of nearly square shape. The top SEM view of Figure 6b applies to
22 samples characterized by 2 μm wide Si trenches and annealed for 5 min. Again, the simulation
23 matches the SEM profiles, revealing that bridging in this case takes place close to the corners of
24 the Ge crystals. This happens because the four top edges are smeared out, producing enough
25 accumulation of material at their sides (see red arrows and Figure S5 in the Supporting
26 Information) to initiate coalescence.
27
28
29
30
31
32
33
34
35
36
37
38
39
40
41
42
43
44
45
46
47
48
49
50
51

52
53 **3.2 Material quality.** So far, the very good agreement between the simulated and experimental
54 evolution towards full coalescence may be considered of mere fundamental interest. Indeed, the
55
56
57
58
59
60

1
2
3 suspended film discussed above resulted from the merging of crystals characterized by extended,
4 flat (001) top facets. As mentioned in the Introduction, this leads to a non-vanishing threading-
5 dislocation density in the top region.^[10] Our final goal, however, is to provide a path leading to
6 virtually dislocation-free suspended Ge films on Si. To this end, it is necessary to form the
7 coalesced film from a set of Ge pillars featuring fully pyramidal top faceting, as found for
8 narrow Si pillars and higher growth temperature shown in Figure 2. In refs [7], [9] and [10] we
9 indeed demonstrated that no threading-dislocations are present in the upper part of the crystals,
10 where the merging induced by annealing begins. Any additional dislocations nucleating during
11 coalescence would therefore have to reside in a cylindrical expanding bridge, which is still
12 surrounded by free surfaces. These free surfaces may, however, be expected to get nucleated
13 defects. As the fully faceted top profile is closer to a rounded shape (see Figure 7a), with smaller
14 curvature gradients, the annealing time for full coalescence is expected to be larger than in the
15 case of more squared profiles (found for larger Si pillars or lower growth temperatures). This is
16 actually confirmed by the simulations reported in Figure 7b,c. From the reported comparison at
17 fixed annealing time and temperature between the evolution of an array of Ge crystals grown at
18 450°C (flat top) and 500°C (pyramidal, fully-faceted top), indeed, it can be seen that coalescence
19 does take place in both cases, but merging is far from completed when starting from a pyramidal
20 shape even after the maximum annealing time (60 minutes) at the maximum temperature
21 (800°C) available in our growth chamber. This was indeed confirmed by experiments, as
22 demonstrated in Figure 8 (center of panel (b)). The following dislocation analysis is therefore
23 limited to a connected network including the expanded cylindrical bridges with a periodic array
24 of small holes, rather than a fully coalesced film. In Figure 8a-b we report the results of an etch-
25 pit analysis by Nomarski interference microscopy (circular enlarged views) after selective defect
26
27
28
29
30
31
32
33
34
35
36
37
38
39
40
41
42
43
44
45
46
47
48
49
50
51
52
53
54
55
56
57
58
59
60

1
2
3 etching (see Experimental Section) on as-grown and 60 min annealed Ge samples. These images
4
5 are combined with top-view SEM images, showing the patterned region close to the planar
6
7 region. We see that etch-pits related to emerging threading dislocations are present in the planar
8
9 region of the as-grown sample (density of $(3 \pm 1) \times 10^8 \text{ cm}^{-2}$), while no etch-pits were found in
10
11 an area of 30×30 Ge crystals (corresponding to a maximum dislocation density of $7 \times 10^4 \text{ cm}^{-2}$).
12
13 After thermal annealing, the etch-pit density in the planar region is lowered by a factor of ~ 30 ,
14
15 while no additional etch-pits appear upon crystal merging in the patterned region of the same
16
17 size as in the as-grown case. This statistically relevant information is supported also by STEM
18
19 and HR-TEM cross-section views, taken along a cut in the [110] direction, passing through the
20
21 centers of the coalescence bridges, as reported in Figure 8c. Here we see that dislocations are
22
23 indeed present close to the bottom of the Ge crystals, whereas only twin defects are seen in a
24
25 columnar distribution in the bridge region. Indeed, small angle grain boundaries must be
26
27 expected to originate from the small random Ge crystal tilts, analyzed in-depth in ref [9]. These
28
29 results show the superior potential of the present technique with respect to other coalescence
30
31 methods widely exploited in group IV or III-V semiconductors, such as Epitaxial Lateral
32
33 Overgrowth (ELO) [21-24], which lead to defected merging regions.
34
35
36
37
38
39
40
41
42

43 **4. CONCLUSION**

44
45 We have demonstrated that a flat, thick suspended Ge layer can be obtained from an array of
46
47 isolated Ge crystals by exploiting surface diffusion of material during annealing. A surface-
48
49 diffusion model based on a phase-field approach was used first to guide experiments and then to
50
51 give an interpretation of the findings. The good agreement between experimental and simulated
52
53 morphologies allowed the full merging process to be attributed to a single, dominating driving
54
55 force: surface-curvature.
56
57
58
59
60

1
2
3 Further optimization in the growth/annealing procedure is still needed in order to obtain
4 continuously flat suspended layers starting from crystals free of any threading dislocation at their
5 tops. Unfortunately, extending the annealing time to a few hours, and/or rising the temperature
6 was not possible in our growth chamber, but our simulations indicate that a flat film is eventually
7 obtained. Ex-situ annealing is also viable, provided that complete Ge oxide removal is
8 performed, and thermal treatment in a suitable atmosphere is operated to maintain a high Ge
9 mobility, still not possible in our laboratory. However, characterization of partially-coalesced
10 films already indicates a promising path to produce suspended Ge layers with low dislocation
11 density, by controlling the merging across engineered nanometric gaps.
12

13
14 Importantly, similar results can be achieved with vertical crystals obtained by growth techniques
15 other than LEPECVD, provided that surface diffusion lengths can be kept at a submicron scale.
16 Finally, preliminary tests indicate that the same merging process can also be applied also to Ge-
17 rich $\text{Si}_{1-x}\text{Ge}_x$ crystals,^[8] to be subsequently topped by a thin Ge layer, the method may also
18 become suitable for the monolithic integration of strained Ge MOSFETs on silicon substrates,
19 the next target of the present technology roadmap of microelectronics.
20
21
22
23
24
25
26
27
28
29
30
31
32
33
34
35
36
37
38
39
40
41
42
43
44

45 ASSOCIATED CONTENT

46
47
48 **Supporting Information.** Further details on phase-field modeling and on the coalescence
49 process, the detailed evolution of large crystals, the role of the anisotropic surface-energy density
50 in the simulated evolutions, plus a full video reporting the evolution shown in Figure 5. This
51 material is available free of charge via the Internet at <http://pubs.acs.org>
52
53
54
55
56
57
58
59
60

AUTHOR INFORMATION

Corresponding Author

*E-mail: leo.miglio@unimib.it

Notes

The authors declare no competing financial interest.

ACKNOWLEDGEMENTS

We are grateful to M. A. Schubert (IHP Frankfurt Oder) for technical support in the STEM analysis, to P. Niedermann (CSEM Neuchatell) for providing the patterned substrates, to D. Chrastina (L-NESS, Politecnico di Milano) for accurately revising the manuscript and to A. Marzegalli (Università di Milano-Bicocca) for helpful discussions on dislocations. We gratefully acknowledge support of Pilegrowth Tech S.r.l. and of the Project NOVIPIX CRSII2_147639 of the Swiss National Science Foundation.

REFERENCES

[1] Dai, X.; Nguyen, B.-M.; Hwang, Y.; Soci, C.; Dayeh, S. A. Novel Heterogeneous Integration Technology of III–V Layers and InGaAs FinFETs to Silicon. *Adv. Funct. Mater.* **2014**, *24*, 4420-4426.

1
2
3 [2] Pillarisetty, R. Academic and industry research progress in germanium nanodevices.
4
5 *Nature* **2011**, 479, 324-328.
6
7

8
9 [3] Currie, M. T.; Samavedam, S. B.; Langdo, T. A.; Leitz, C. W.; Fitzgerald, E. A.
10 Controlling threading dislocation densities in Ge on Si using graded SiGe layers and chemical-
11 mechanical polishing *Appl. Phys. Lett.* **1998**, 72, 1718-1720.
12
13

14
15 [4] Park, J-S.; Bai, J.; Curtin M.; Adekore, B.; Carroll, M.; Lochtefeld, A. Defect reduction
16 of selective Ge epitaxy in trenchus on Si(001) substrates using aspect ratio trapping. *Appl. Phys.*
17 *Lett.* **2007**, 90, 052113.
18
19

20
21 [5] Wang, G.; Rosseel, E.; Loo, R.; Favia, P.; Bender, H.; Caymax, M.; Heyns, M. M.;
22 Vandervorst, W. High quality Ge epitaxial layers in narrow channels on Si (001) substrates.
23 *Appl. Phys. Lett.* **2010**, 96, 111903.
24
25

26
27 [6] Hudait, M. K.; Clavel M.; Goley, P.; Jain N.; Zhu Y. Heterogeneous Integration of
28 Epitaxial Ge on Si using AlAs/GaAs Buffer Architecture: Suitability for Low-power Fin Field-
29 Effect Transistors. *Sci. Rep.* **2014**, 4, 6964.
30
31

32
33 [7] Falub, C. V.; von Känel, H.; Isa F.; Bergamaschini, R.; Marzegalli, A.; Chrastina, D.;
34 Isella, G.; Müller E.; Niedermann, P.; Miglio, L. Scaling Hetero-Epitaxy from Layers to Three-
35 Dimensional Crystals. *Science* **2012**, 335, 1330-1334.
36
37

38
39 [8] Bergamaschini, R.; Isa, F.; Falub, C. V.; Niedermann, P.; Müller, E.; Isella, G.; von
40 Känel, H.; Miglio, L. Self-Aligned Ge and SiGe Three-Dimensional Epitaxy on Dense Si Pillar
41 Arrays. *Surf. Sci. Rep.* **2013**, 68, 390-417.
42
43
44
45
46
47
48
49
50
51
52
53
54
55
56
57
58
59
60

1
2
3 [9] Falub, C. V.; Meduňa, M.; Chrastina, D.; Isa, F.; Marzegalli, A.; Kreiliger, T.; Taboada,
4 A.G.; Isella, G.; Miglio, L.; Dommann, A.; von Känel, H. Perfect crystals grown from imperfect
5 interfaces. *Sci. Rep.* **2013**, *3*, 2276.
6
7

8
9
10
11 [10] Marzegalli, A.; Isa, F.; Groiss, H.; Müller, E.; Falub, C. V.; Taboada, A. G.; Niedermann,
12 P.; Isella, G.; Schäffler, F.; Montalenti, F.; von Känel, H., Miglio, L. Unexpected Dominance of
13 Vertical Dislocations in High-Misfit Ge/Si(001) Films and Their Elimination by Deep Substrate
14 Patterning. *Adv. Mater.* **2013**, *25*, 4408-4412.
15
16
17

18
19
20
21 [11] Rosenblad, C.; Deller, H. R.; Dommann, A.; Meyer, T.; Schroeter, P.; von Känel, H.
22 Silicon epitaxy by low-energy plasma enhanced chemical vapor deposition. *J. Vac. Sci. Technol.*
23 *A* **1998**, *16*, 2785.
24
25
26
27

28
29
30 [12] Kern, W. ; Puotinen, D. A. Cleaning solutions based on hydrogen peroxide for use in
31 silicon semiconductor technology. *RCA Rev.* **1970**, *31*, 187-206.
32
33

34
35 [13] Marchionna, S.; Virtuani, A.; Acciarri, M.; Isella, G.; von Känel, H. Defect imaging of
36 SiGe strain relaxed buffers grown by LEPECVD. *Mater. Sci. Semicond. Process.* **2006**, *9*, 802-
37 805.
38
39
40

41
42
43 [14] Li B.; Lowengrub J.; Ratz A. and Voigt A. Geometric Evolution Laws for Thin
44 Crystalline Films: Modeling and Numerics. *Comm. Comput. Phys.* **2009**, *6*, 433-482.
45
46

47
48 [15] Salvalaglio, M.; Backofen, R.; Bergamaschini, R.; Montalenti, F.; Voigt, A. Faceting of
49 Equilibrium and Metastable Nanostructures: A Phase-Field Model of Surface Diffusion Tackling
50 Realistic Shapes. *Cryst. Growth Des.* **2015**, *15*, 2787-2794.
51
52
53
54
55
56
57
58
59
60

1
2
3 [16] Huang L.; Liu F.; Lu G.-H.; Gong. X. G. Surface Mobility Difference between Si and Ge
4 and Its Effect on Growth of SiGe Alloy Films and Islands. *Phys. Rev. Lett.* **2006**, 96, 016103.
5
6

7
8
9 [17] Vey S.; Voigt A. AMDiS: Adaptive Multidimensional Simulations. *Comput. Visual. Sci.*
10 **2006**, 10, 57-67.
11
12

13
14 [18] Witkowski, T.; Ling, S.; Praetorius, S.; Voigt, A. Software concepts and numerical
15 algorithms for a scalable adaptive parallel finite element method. *Adv. Comput. Math.* **2015**.
16
17

18
19
20 [19] Uberuaga B. P.; Leskovar M.; Smith A. P.; Jonsson H.; Olmstead M. Diffusion of Ge
21 below Si(100) Surface: Theory and Experiment. *Phys. Rev. Lett.* **2000**, 84, 2441-2444
22
23

24
25 [20] Mullins, W. W. Theory of Thermal Grooving. *J. Appl. Phys.* **1957**, 28, 333-339.
26
27

28
29 [21] Gupta, A; Jacob, C. Selective epitaxy and lateral overgrowth of 3C-SiC on Si – A review.
30 *Prog. Cryst. Growth Charact. Mater.* **2005**, 51, 43-69.
31
32

33
34 [22] Kim, S.W; Cho, Y. D.; Park, W. K.; Kim, D. H.; Ko, D.H. Defect analyses of selective
35 epitaxial grown GaAs on STI patterned (001) Si substrates. *J. Cryst. Growth* **2014**, 401, 319-322.
36
37

38
39 [23] Kim, B.; Kim S.-W.; Jang, H.; Kim, J.-H.; Koo, S.; Kim, D.-H; Min, B.-G.; Park, S.-J.,
40 Song; J. S., Ko, D.-H. Strain evolution during the growth of epitaxial Ge layers between narrow
41 oxide trenches. *J. Cryst. Growth* **2014**, 401, 308-313.
42
43
44

45
46 [24] Leonhardt, D; Sheng, J.; Cederberg, J. G.; Qiming, L.; Carrol, M. S.; Sang M. H.
47 Nanoscale interfacial engineering to grow Ge on Si as virtual substrates and subsequent
48 integration of GaAs. *Thin Solid Films* **2010**, 518, 5920-5927.
49
50
51
52
53
54
55
56
57
58
59
60

FIGURES

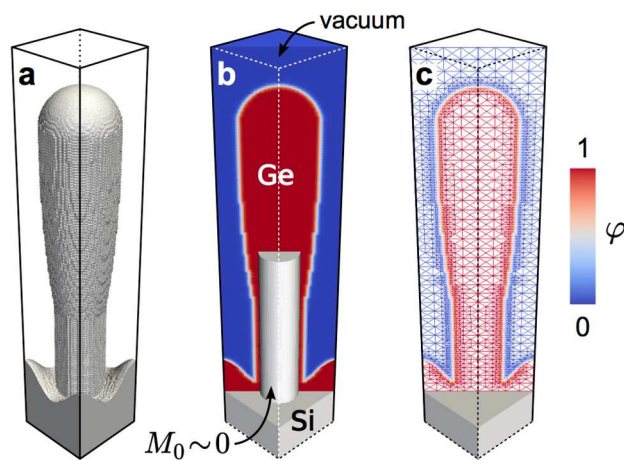


Figure 1. Phase-field modeling. a) 3D view of the simulation cell embedding a pillar-like structure implicitly defined according to the phase-field approach. The profile corresponds to the iso-surface at $\varphi = 0.5$. b) Cross-section of the cell showing the variation of φ from the solid region to the vacuum. The 3D grey region corresponds to the immobile Si pillar ($M_0 \sim 0$). c) Mesh structure with local refinement at the surface of the solid phase, i.e. at $\varphi = 0.5$. The color map reports the values of φ .

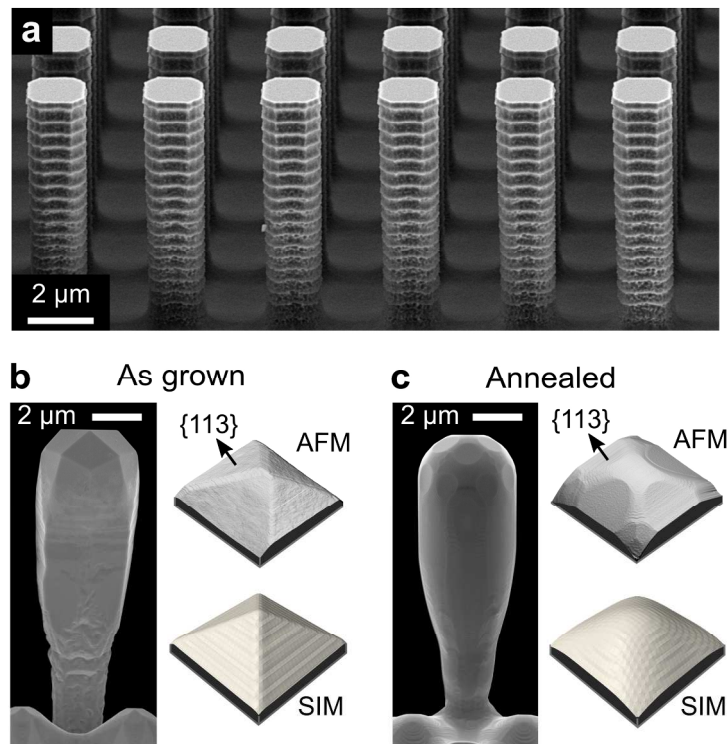


Figure 2. Growth and annealing of individual crystals. a) SEM lateral view of a pattern formed by $2 \times 2 \mu\text{m}^2$ wide Si pillars with $2 \mu\text{m}$ trench prior to deposition. SEM lateral views and AFM perspective views of the crystal top are shown: b) as-grown $8 \mu\text{m}$ tall Ge crystal obtained by deposition at $500 \text{ }^\circ\text{C}$ on a Si substrate patterned with $8 \mu\text{m}$ tall and $2 \times 2 \mu\text{m}^2$ wide pillars, spaced by $3 \mu\text{m}$ trenches; c) in-situ annealing of the structure in panel (b) by six thermal cycles ranging from 600 to $800 \text{ }^\circ\text{C}$. The top morphology in (c), is compared with the profile resulting from a phase-field simulation (“SIM”) of surface diffusion starting from the as-grown geometry, as sketched in the inset of panel (b).

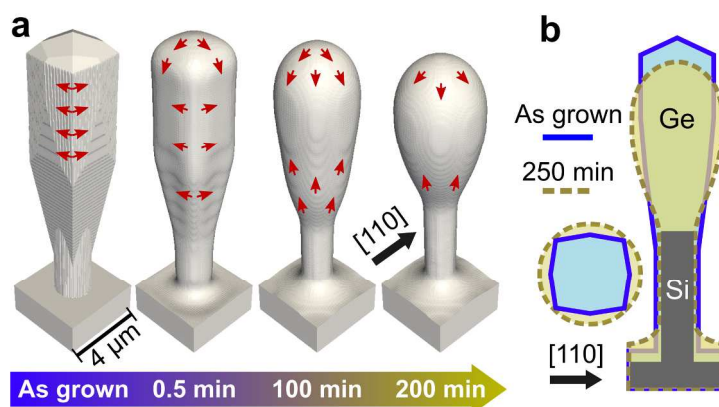


Figure 3. Simulation of annealing of an isolated crystal. a) phase-field simulation of the profile evolution of an isolated crystal, starting from the as-grown geometry shown in Figure 2b. Illustrative arrows show the material fluxes given by the local curvature. b) Cross- and top-view comparison between the first and the last simulation profile in panel (a).

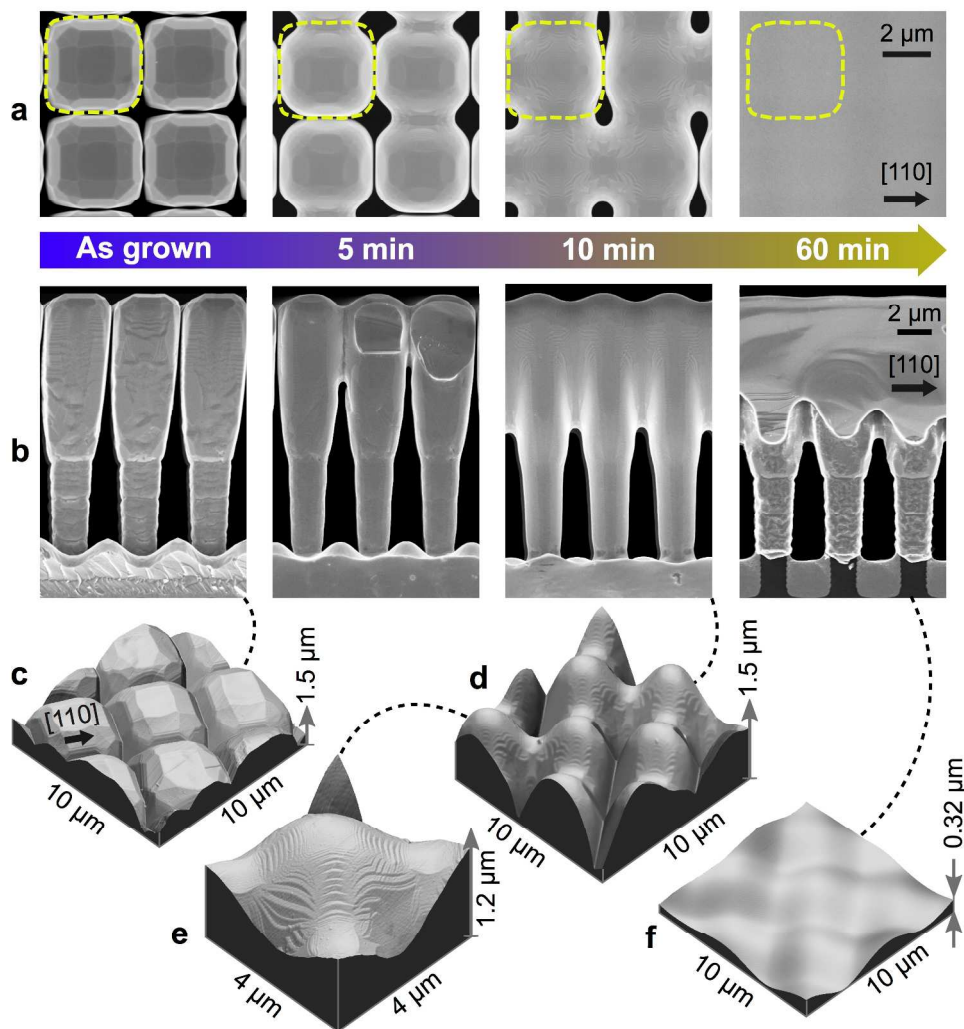


Figure 4. Coalescence process induced by annealing. a) top and b) lateral SEM views of Ge crystals grown at 450 °C on 8 μm tall and $2 \times 2 \mu\text{m}^2$ wide Si pillars separated by 2 μm trenches after in-situ annealing experiments of different durations at 800 °C. AFM views of the samples reported in panel (a) and (b) are shown: c) as-grown; d) after annealing for 10 min; e) magnification of the top of a fused crystal in (d), revealing the existence of stepped regions along the facets; f) after annealing for 60 min.

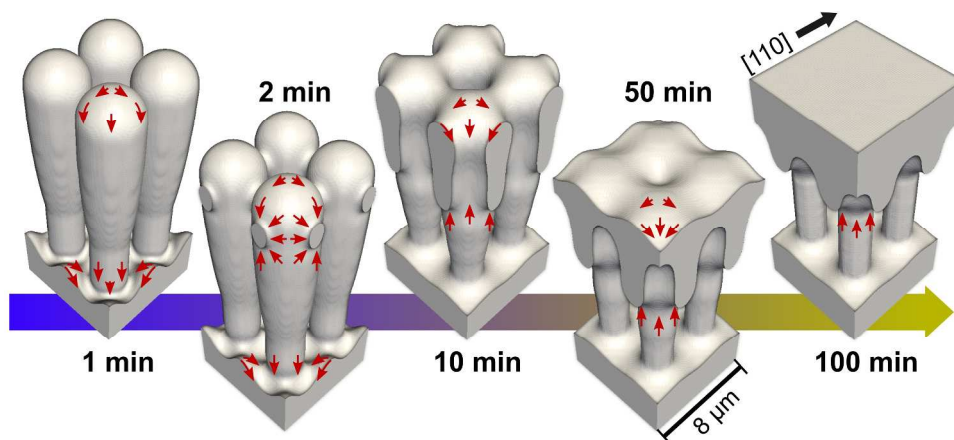


Figure 5. Phase-field simulations of the coalescence process. Snapshots of the phase-field simulation matching the main features of the annealing experiments shown in Figure 4 (a movie showing the whole evolution is provided in the Supporting Information).

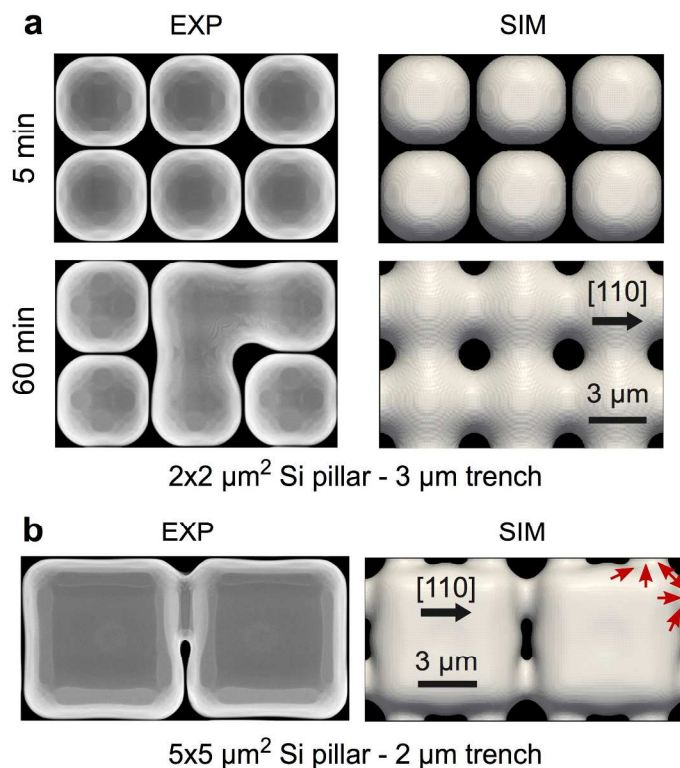


Figure 6. Features of the coalescence process. a) SEM (left, “EXP”) and simulation (right, “SIM”) top views of samples obtained after annealing for 5 and 60 min of 8 μm tall Ge crystals grown at 450 °C on 8 μm tall and 2×2 μm² wide Si pillars, spaced by 3 μm trenches. b) SEM (left) and simulation (right) top views of samples obtained after annealing for 5 min of 8 μm tall Ge crystals grown at 450 °C on 8 μm tall and 5×5 μm² large Si pillars, spaced by 2 μm trenches. Illustrative arrows in panel (b) show the material fluxes in a representative region.

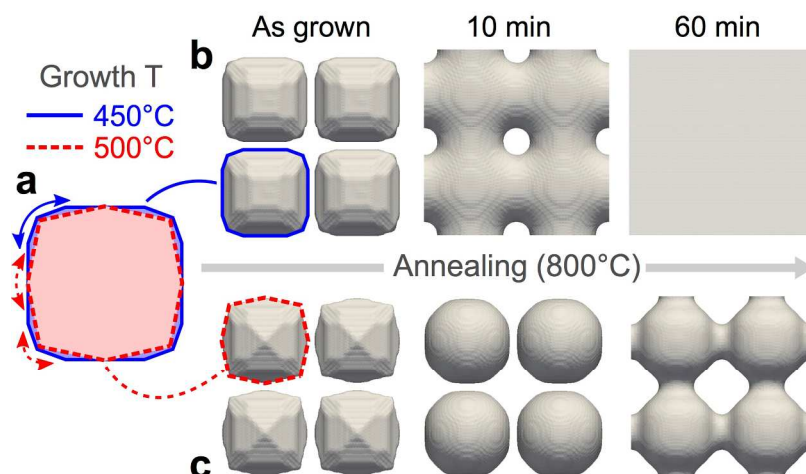


Figure 7. Influence of the as-grown morphology. a) Comparison between the top sections of Ge crystals grown at 450°C (solid blue line) and 500°C (dashed red line). b, c) Simulation results of the evolution driven by surface diffusion resulting from the two different initial top morphologies in panel (a). The same mobility coefficient M_0 used in the simulation of Figure 6 is considered for both cases (b, c). In agreement with experiments, the coalescence process is delayed for the structure grown at high temperature (b).

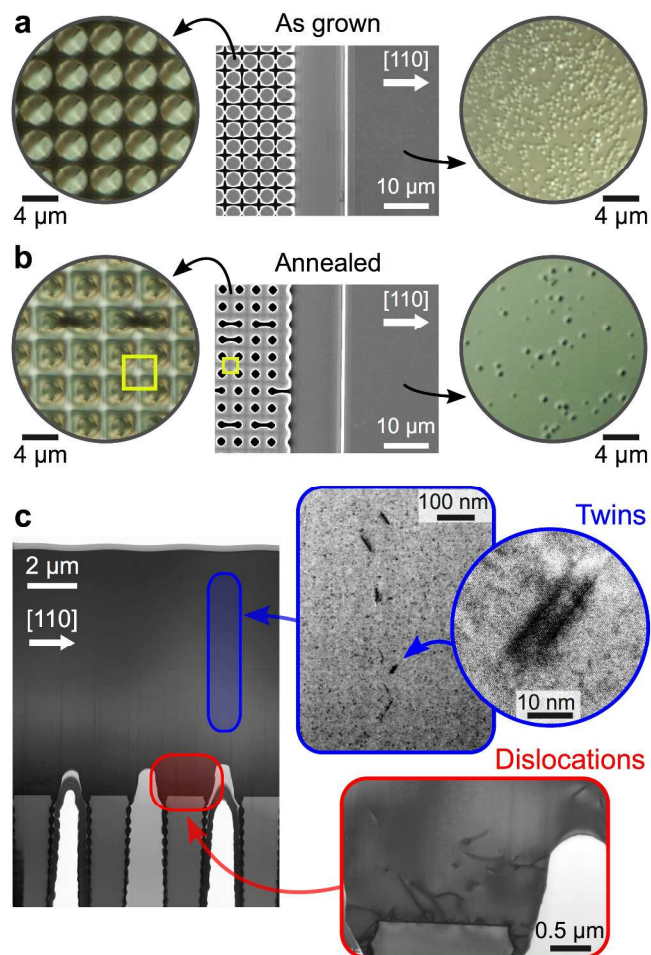
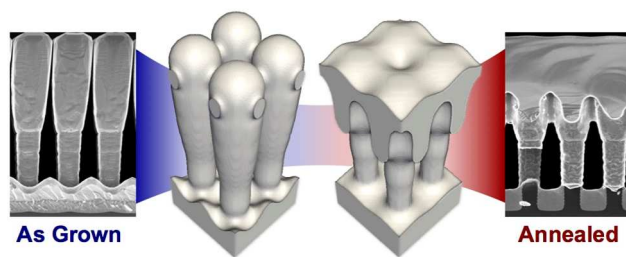
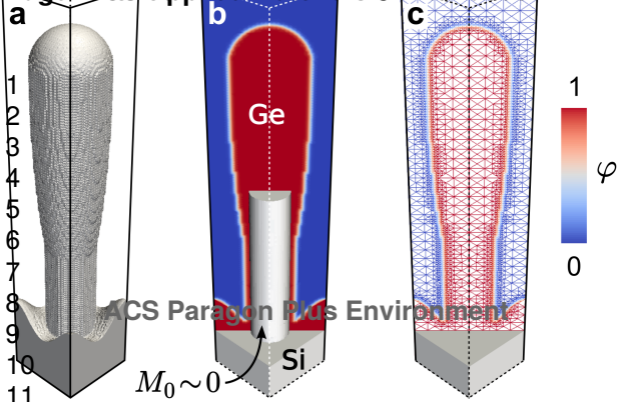


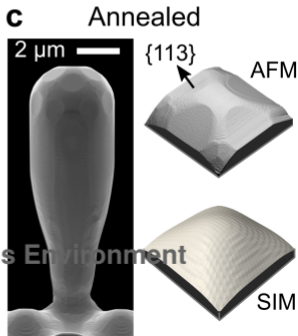
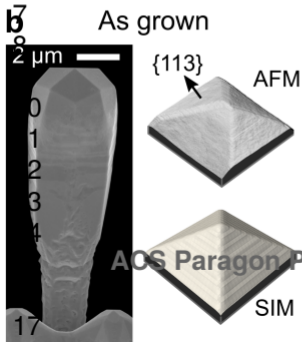
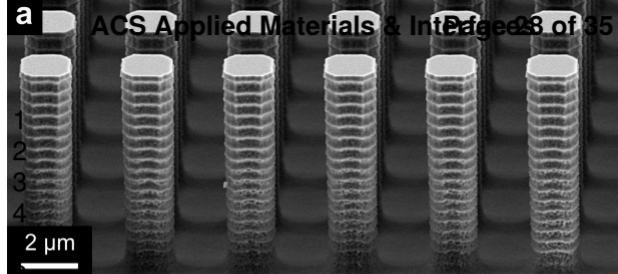
Figure 8. Quality of the coalesced structure. a, b) Etch-pit analysis shown by SEM and Nomarski microscopy (circular enlarged views). Both planar unpatterned and patterned regions, the latter corresponding to $2 \times 2 \mu\text{m}^2$ wide $8 \mu\text{m}$ tall Si pillars spaced by $2 \mu\text{m}$ trenches, are considered. Samples obtained by $8 \mu\text{m}$ Ge deposition at $500 \text{ }^\circ\text{C}$ are shown before (a) and after (b) in-situ annealing by six thermal cycles as reported in Figure 2. c) STEM bright-field cross-section of the sample in panel (b). Insets show magnifications of both twins and dislocations obtained by bright-field HR-TEM.

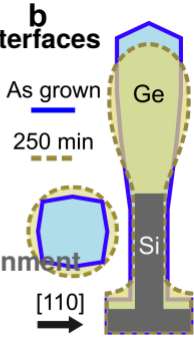
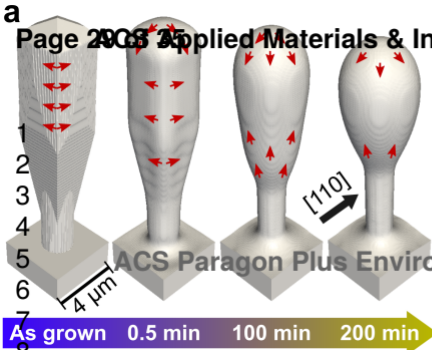
1
2
3
4
5
6
7
8
9
10
11
12
13
14
15
16
17
18
19
20
21
22
23
24
25
26
27
28
29
30
31
32
33
34
35
36
37
38
39
40
41
42
43
44
45
46
47
48
49
50
51
52
53
54
55
56
57
58
59
60

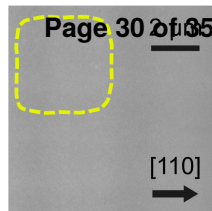
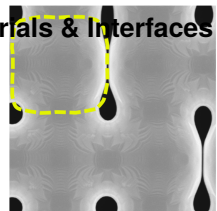
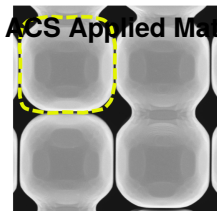
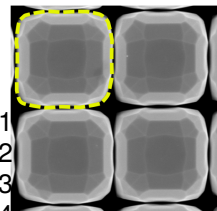
Graphic Table of Contents









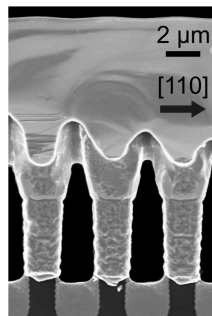
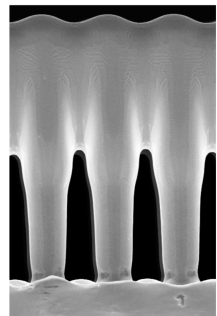
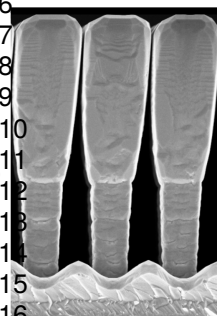
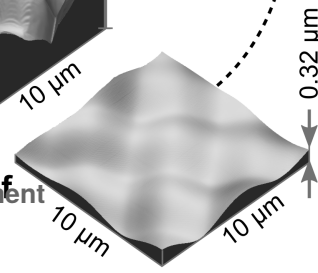
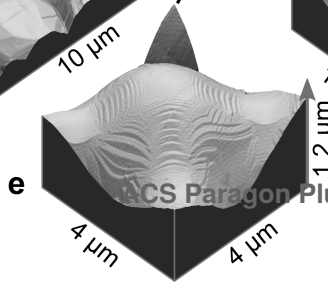
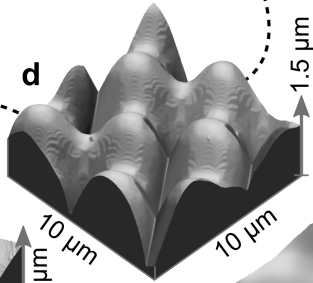
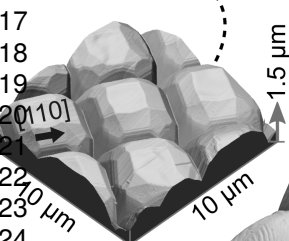
a
1
2
3
4

As grown

5 min

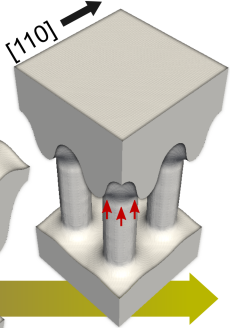
10 min

60 min

b
6
7
8
9
10
11
12
13
14
15
16c
17
18
19
20
21
22
23
24
25
26
27
28
29
30

2 min

50 min



1
2
3
4
5
6
7
8
9
10

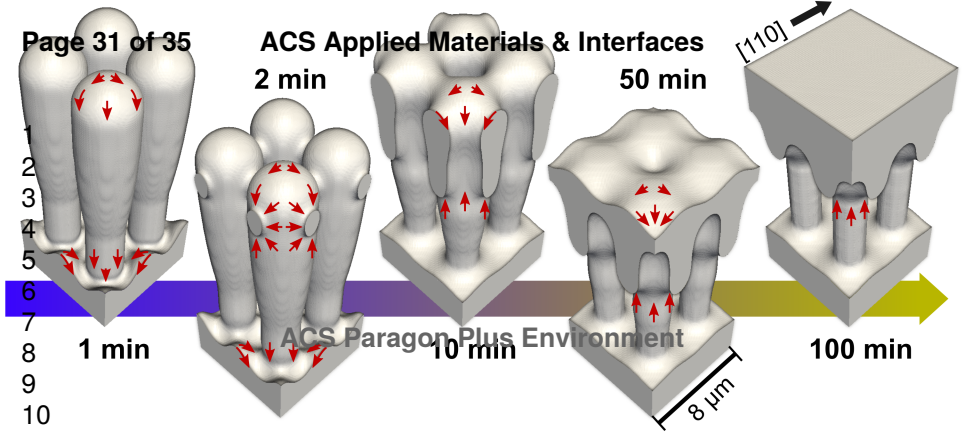
1 min

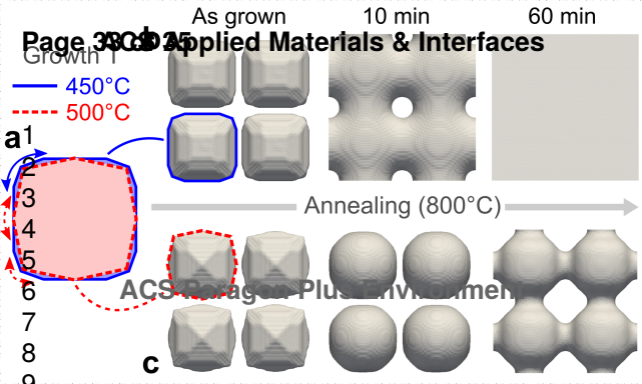
10 min

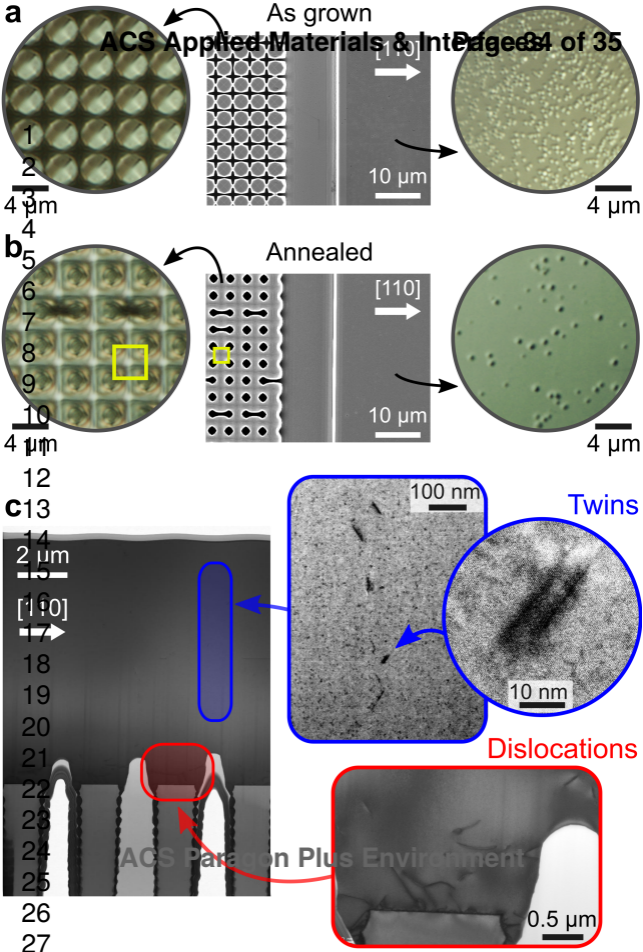
100 min

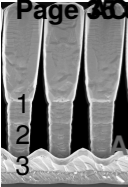
ACS Paragon Plus Environment

8 μm

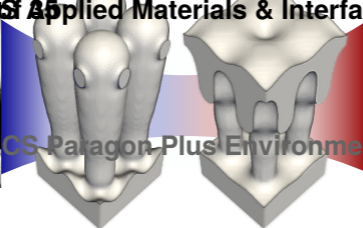




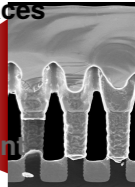




As Grown



ACS Paragon Plus Environment



Annealed